# Insights into the product release mechanism of dengue virus NS3 helicase

**Natalia S. Adler[1,2,†], Leila A. Cababie[3,4,†], Carolina Sarto[5,9], Claudio N. Cavasotto[2,7,8], Leopoldo G. Gebhard[10], Darío A. Estrin[5,6], Andrea V. Gamarnik[11], Mehrnoosh Arrar[12,*] and Sergio B. Kaufman [ORCID][3,4,*]**

[1]CONICET, Centro de Investigaciones en Bionanociencias (CIBION), Buenos Aires, B1630FHB Argentina, [2]CONICET-Universidad Austral, Instituto de Investigaciones en Medicina Traslacional (IIMT), Pilar, Buenos Aires, B1630FHB Argentina , [3]CONICET-Universidad de Buenos Aires, Instituto de Química y Físicoquímica Biológica (IQUIFIB), Buenos Aires, C1113AAD Argentina, [4]Universidad de Buenos Aires, Facultad de Farmacia y Bioquímica, Departamento de Química Biológica, Buenos Aires, C1113AAD Argentina, [5]Universidad de Buenos Aires, Facultad de Ciencias Exactas y Naturales, Departamento de Química Inorgánica, Analítica y Química Física, Buenos Aires, C1428EGA Argentina, [6]CONICET-Universidad de Buenos Aires, Instituto de Química Física de los Materiales, Medio Ambiente y Energía (INQUIMAE), Buenos Aires, C1428EGA Argentina, [7]Universidad Austral, Facultad de Ciencias Biomédicas, and Facultad de Ingeniería, Pilar, Buenos Aires, B1630FHB Argentina, [8]Universidad Austral, Austral Institute for Applied Artificial Intelligence, Pilar, Buenos Aires, B1630FHB Argentina, [9]CONICET-Universidad de Buenos Aires, Instituto de Química Biológica de la Facultad de Ciencias Exactas y Naturales (IQUIBICEN), Buenos Aires, C1428EGA Argentina, [10]CONICET-Universidad Nacional de Quilmes, Departamento de Ciencia y Tecnología, Bernal, Buenos Aires, B1876 Argentina, [11]Fundación Instituto Leloir- CONICET, Buenos Aires, C1405BWE Argentina and [12]CONICET-Universidad de Buenos Aires, Instituto de Cálculo, Buenos Aires, C1428EGA Argentina

## ABSTRACT

**The non-structural protein 3 helicase (NS3h) is a multifunctional protein that is critical in RNA replication and other stages in the flavivirus life cycle. NS3h uses energy from ATP hydrolysis to translocate along single stranded nucleic acid and to unwind double stranded RNA. Here we present a detailed mechanistic analysis of the product release stage in the catalytic cycle of the dengue virus (DENV) NS3h. This study is based on a combined experimental and computational approach of product-inhibition studies and free energy calculations. Our results support a model in which the catalytic cycle of ATP hydrolysis proceeds through an ordered sequential mechanism that includes a ternary complex intermediate (NS3h-Pi-ADP), which evolves releasing the first product, phosphate (Pi), and subsequently ADP. Our results indicate that in the product release stage of the DENV NS3h a novel open-loop conformation plays an important role that may be conserved in NS3 proteins of other flaviviruses as well.**

## INTRODUCTION

Non-structural protein 3 (NS3) is a multifunctional viral protein that is critical (1) in the dengue virus (DENV) life cycle, specifically implicated in viral replication, encapsidation, host immune evasion, and processing of the polyprotein precursor (2,3). The N-terminal region of NS3 is characterized as a serine protease, whereas the C-terminal region is classified as an RNA helicase, which also has NTPase, RTPase and RNA annealing activities (4–7).

In particular, the NS3 helicase (NS3h) is an energy transducer or molecular motor that translocates along single-stranded and unwinds double-stranded RNA, while catalyzing the hydrolysis of nucleoside triphosphates (NTPs). It couples an energetic-catalytic cycle comprised of the hydrolysis of NTPs to a mechanical work cycle consisting of a sequence of transitions of double-stranded RNA unwinding/translocation along single-stranded nucleic acid.

A current hypothesis to explain such coupling is that successive energy states (conformational states) during the hydrolysis of NTPs at the protein catalytic site propagate through the protein structure producing the mechanical movements of translocation at the nucleic acid binding site. A molecular description of the transduction mechanism requires identifying and characterizing all intermediate states of both cycles as well as establishing the synchronization between phases of the mechanical movement and each step of the catalytic cycle.

The DENV NS3h is phylogenetically characterized within the DExH/D subgroup of the monomeric SF2 helicases. Within this subgroup, the DEAD-box and DExH helicases can be further distinguished, according to biochemical and kinetic analysis. Though the DENV NS3h (sequence motif DEAH) is structurally similar to the DExH helicases, which include the closely related and extensively studied NS3h of the Hepatitis C Virus (HCV), it is similar to the DEAD-box helicases in terms of its inefficient unwinding of double-stranded DNA (8,9) and lack of processivity as an RNA helicase (9,10).

The DENV NS3h is structurally organized in three sub-domains; the core of the molecular motor is comprised of two RecA-like domains (D1 and D2), which form the NTP-binding cleft on one side and an RNA-binding interface on the opposite side. A third sub-domain (D3) further secures ssRNA (Figure 1). The DENV NS3h has been crystallized both in presence and absence of ssRNA, in various nucleotide-binding conditions (11). In contrast to crystallographic studies of the HCV NS3h, the structures of the DENV NS3h did not evidence major conformational changes in the different nucleotide-binding conditions.

In previous work (12), we performed classical molecular dynamics (MD) simulations of the DENV NS3h in different nucleotide-bound states along the ATP-hydrolysis cycle, namely NS3h:RNA, NS3h:RNA:ATP and NS3h:RNA:ADP:Pi, where the initial configurations were taken from 2jlu, 2jlv and 2jly PDB IDs, respectively (11). In this previous study, we observed greater structural fluctuations of the protein backbone in the product-bound state, despite a similar average conformation to that of the ATP-bound state. Among these fluctuations, we identified a novel open-loop conformation of the DENV NS3h, which not only distinguishes both the free and product-bound states from the ATP-bound state, but also highlights a plausible alternative exit channel (backdoor channel) for Pi from the catalytic site of the enzyme (Figure 1).

As a contribution to the general study of the energy transduction process mentioned above, we determined the mechanism of product release from the catalytic cycle of the hydrolysis of ATP by DENV NS3h. We used two independent approaches to study this process: on the one hand, following the steady state kinetics of ATP hydrolysis by NS3h in the presence of products and, on the other, computationally calculating free energy profiles of the release of Pi and ADP from the catalytic site of the enzyme.

Our results support an ordered sequential mechanism of product release in which Pi is the first product to be released and ADP the second. Free energy profiles constructed from biased MD simulations further support this model and suggest that the open-loop conformation plays a key role in facilitating Pi release.

## MATERIALS AND METHODS

### General reagents and reaction conditions

KCl, MgCl$_2$, KOH and 3-(*N*-morpholino) propanesulfonic acid (MOPS) were provided by Mallinckrodt Baker (ACS reagents). NaOH and HCl were supplied by Carlo Erba. Ethylenediaminetetraacetic acid (EDTA) was obtained from Sigma Aldrich and [(3-cholamidopropyl) dimethylammonio]-1-propanesulfonate (CHAPS) was provided by Thermo-scientific. Nucleotides adenosine 5′-triphosphate (ATP) and adenosine 5′-diphosphate (ADP) were provided by Sigma lyophilized in the di- or tri-sodium salt form. Adenosine triphosphate, labeled on the gamma phosphate group with $^{32}$P-[γ-$^{32}$P]ATP was obtained from PerkinElmer Inc. Potassium phosphate, monobasic (Pi) was supplied by J.T. Baker™. Nucleotide concentrations were determined spectrophotometrically using extinction coefficients taken from literature (13).

Experiments were carried out in the presence of 10 nM of NS3h at 25°C and pH 6.5 in media containing 25 mM MOPS/KOH, 0.5 mM EDTA and 0.5 mM CHAPS (buffer BK). In addition, the reaction medium contained enough KCl, NaCl and MgCl$_2$ to obtain a final concentration of 100 mM K$^+$, 10 mM Na$^+$ and 1.5 mM free Mg$^{2+}$, respectively. To ensure the 1.5 mM free Mg$^{2+}$ concentration in all experimental conditions, the reaction media were prepared by mixing different proportions of stock solutions of ATP, ADP, and Pi. Each stock solution was initially prepared with buffer, salts, EDTA and a total amount of MgCl$_2$ such that, after stoichiometric complexation with the total EDTA present, the equilibrium constant of the corresponding Mg complexes (14) (MgATP, MgADP or MgPi) indicated a free Mg$^{2+}$ concentration of 1.5 mM.

### Protein purification

A construct encoding the helicase domain of NS3 (residues 171–618) was derived from the cDNA of an infected clone of DENV serotype 2 (GenBank accession number U87411) (15). The construct was cloned into vector pET-28a (Novagen, Madison, USA) to obtain plasmid pET-NS3h that was used for high-level expression of N-terminal hexa-histidine-tagged recombinant protein in *Escherichia coli* (6). Protein expression and purification procedures were identical as those described in a previous report (6). Homogeneity of protein preparations was assessed by sodium dodecyl sulphate-polyacrylamide gel electrophoresis and Coomassie Brillant Blue staining. The concentration of enzyme in stock aliquots was calculated from the absorbance at 280 nm and its empirical extinction coefficient in the dialysis buffer (50 mM HEPES–KOH, pH 7.0, 5% v/v glycerol, 200 mM KCl, 0.20 mM DTT), $\epsilon_{280\,nm,25°C} = 70.9$ mM$^{-1}$ cm$^{-1}$ which, in turn, was obtained by the Edelhoch method (16).
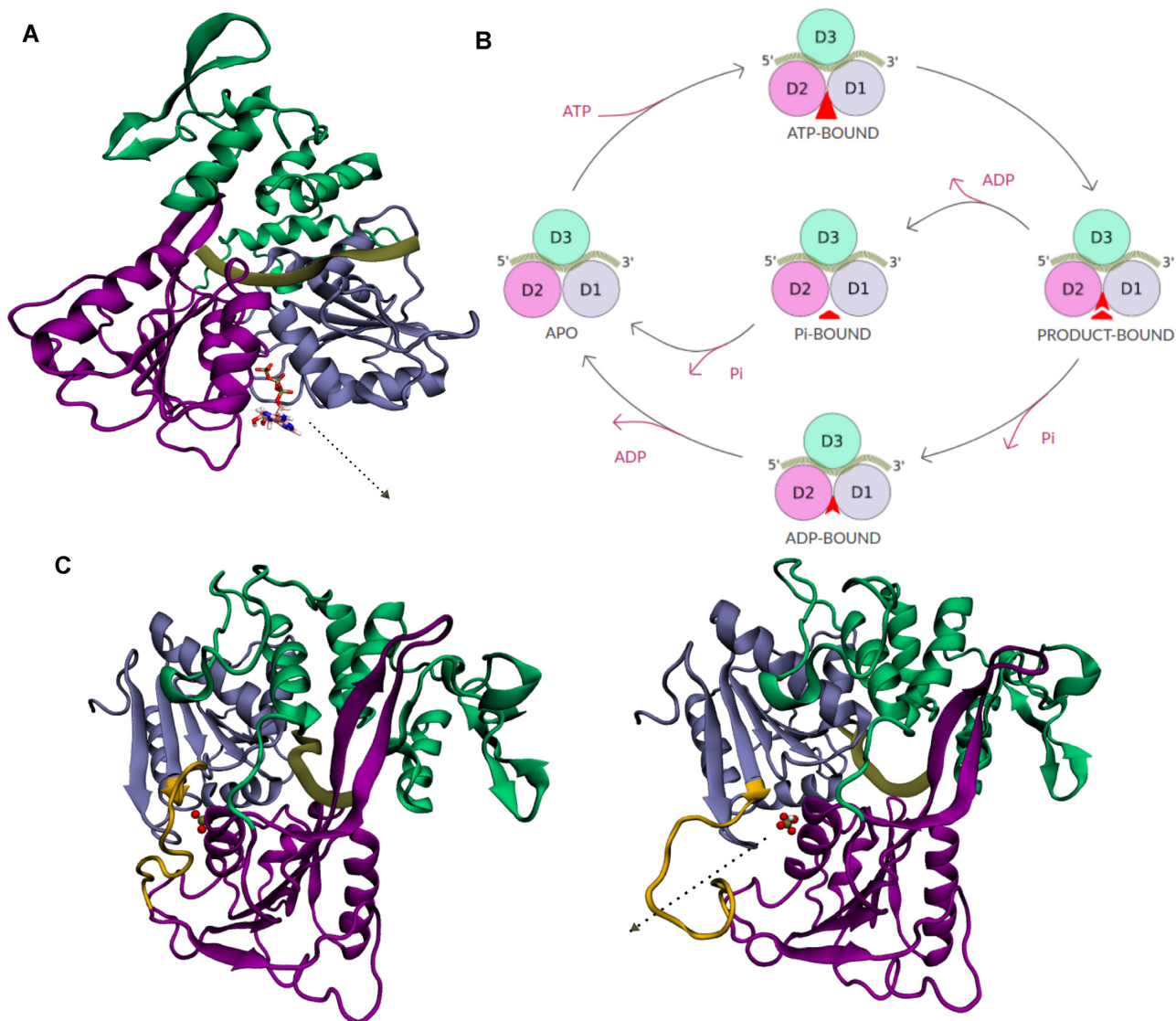
**Figure 1.** Overview of NS3h structure. (**A**) NS3h subdomains are color-coded with the RecA-like motor domains D1 and D2 in purple and magenta, respectively, and D3 in green. Bound ssRNA segment is shown as a tan ribbon, and bound ATP is shown as sticks. (**B**) Deterministic model of ATP hydrolysis cycle, highlighting the two possible release sequences of ADP and Pi. (**C**) NS3h structure is shown rotated 90 about the vertical axis in panel A. β6−β1′ loop is highlighted in gold to distinguish closed-loop (left) and open-loop (right) conformations. Canonical and backdoor channels are indicated with arrows in panels A and C, respectively.

## ATPase activity measurement

ATPase activity was determined according to Schwarzbaum *et al.* (17), measuring the amount of [$^{32}$P]Pi released from [γ-$^{32}$P]ATP. Additional controls for the use of this method in the presence of varying concentrations of Pi and ADP are provided in SI Supplementary Figures S1 and S2.

Briefly, after incubation of 0.25 ml of reaction mixture at 25°C, ATP hydrolysis was stopped by the addition of 500 μl of a solution containing $(NH_4)MoO_4$, 1.25% (w/v) in 5% (v/v) perchloric acid. Immediately after, 500 μl of isobutanol was added and the mixture was vigorously stirred for 25 s and then spun down for 3 min at 1700 × g. In this way, all the phosphomolybdic complex formed was ex-

tracted to the organic phase. Because the Cerenkov emissions, which are mostly in the UV range, also extend into the blue region of the visible spectrum, the yellow color of the phosphomolybdic complex solution is particularly problematic as it absorbs part of these emissions. To avoid this quenching phenomenon, we transferred 250 μl of the organic phase to a tube containing 750 μl of an 8 M NaOH solution, which results in the disintegration of the phosphomolybdic complex, thus resulting in a colorless solutions.

Finally, taking advantage of the Cerenkov effect, radioactivity of the [$^{32}$P]Pi extracted was measured in a liquid scintillation counter (RackBeta 1214) and, from this value, the amount of inorganic phosphate released from hydrolyzed

ATP was calculated (further detail can be found in SI Supplementary Figures S3 and S4).

The initial rate of ATP hydrolysis was obtained from the slope of the time course of phosphate release. At least four different reaction times were used to estimate the velocity and the hydrolysis never exceeded 10% of the ATP present to ensure initial rate conditions. All reactions were initiated with the addition of the enzyme or ATP to the reaction mixture and stopped by the addition of ammonium heptamolybdate solution in acidic medium.

### Data analysis and development of theoretical models

Symbolic solutions of steady state rate equations for different kinetic mechanisms were obtained using the solve simultaneous equations routine of GNU Octave, version 5.1.0. Equations were fitted to the data by nonlinear regression analysis using Libreoffice 3.4.4 spreadsheets. The Akaike Information Criterion (AIC) was used to select among different kinetic models [18]. Figures were edited in QtiPlot version 0.9.8.9.

### Initial configurations MD simulations

Initial snapshots for the first steps of product release were taken from molecular dynamics (MD) simulations from our previous work, with the protein in either the closed-loop or open-loop conformation. Because the open-loop conformation was identified in simulations in which the DENV NS3h was bound to RNA, we modeled the RNA-free state of the open-loop conformation by removing RNA from the MD snapshot, and slowly equilibrating the system over 50 ns. After confirming that the open-loop conformation was also stable in the absence of RNA, an arbitrary snapshot was chosen.

In the case of ADP-$Mn^{2+}$ release as the second step of the product release mechanism, we performed a classical MD simulation of the post-Pi-release state to first equilibrate the system. We then selected arbitrary snapshots from different replicas to model the closed and open-loop conformations for ADP-$Mn^{2+}$ pulling.

For each system, a 5-ns classical MD simulation was performed and 500 snapshots were saved at 10-ps intervals as starting points for independent steered molecular dynamics (SMD) simulations. To ensure the same initial value of the reaction coordinate for every pulling simulation, the coordinates of the ADP molecule and the P atom of the Pi molecule were constrained during the simulation. The same system parameters were used as described previously [12], with minor modifications to the Pi parameters to ensure stability during SMD simulations (see SI).

### Steered MD simulations

The SMD atoms, to which the external harmonic force was applied, were defined as either the P atom of the Pi molecule, or the center of mass of the ADP molecule. In both cases, a pulling vector $\vec{n}$ was defined from the initial coordinates of the respective SMD atom to an arbitrary endpoint such that the vector best represented the channel to be sampled, either canonical or backdoor; reference coordinates and vectors are provided in SI.

The reaction coordinate was defined as the projection of the difference vector between the Cartesian coordinates of the SMD atoms $\vec{r}$ from their initial coordinates $\vec{r_0}$ onto the pulling vector $\vec{n}$. The center of the external harmonic force $f$ varied linearly in time, according to a constant pulling velocity $v$, as shown in Equation (1):

$$f = \frac{1}{2}k[vt - (\vec{r} - \vec{r_0})\vec{n}]^2 \tag{1}$$

where $k$ is the force constant. A force constant of 70 kcal/mol/$\mathring{A}^2$ was used for all simulations. For Pi pulling, a velocity of 0.001 Å/timestep was used; for ADP pulling a velocity of 0.0001 and 0.00005 Å/timestep was used for closed and open conformations, respectively. The ILE 281 Cα and $Mn^{2+}$ atom that were constrained in the generation of the initial configurations remained constrained during the SMD simulations, to maintain the orientation of the system and limit sampling errors; except in the case of ADP-$Mn^{2+}$ release where the GLN 277 Cα atom was constrained instead of the $Mn^{2+}$ atom. All simulations were carried out using the NAMD software [19]. The overall distance that the SMD atoms were pulled varied for each system, depending on when the free energy profile (FEP) leveled off. In each case we verified that the product species being released had indeed dissociated from the product complex. Additional FEPs were constructed from the dissociated product state to ensure no additional barriers in migration to the solvent (Supplementary Figure S6 SI).

### Construction of free energy profiles

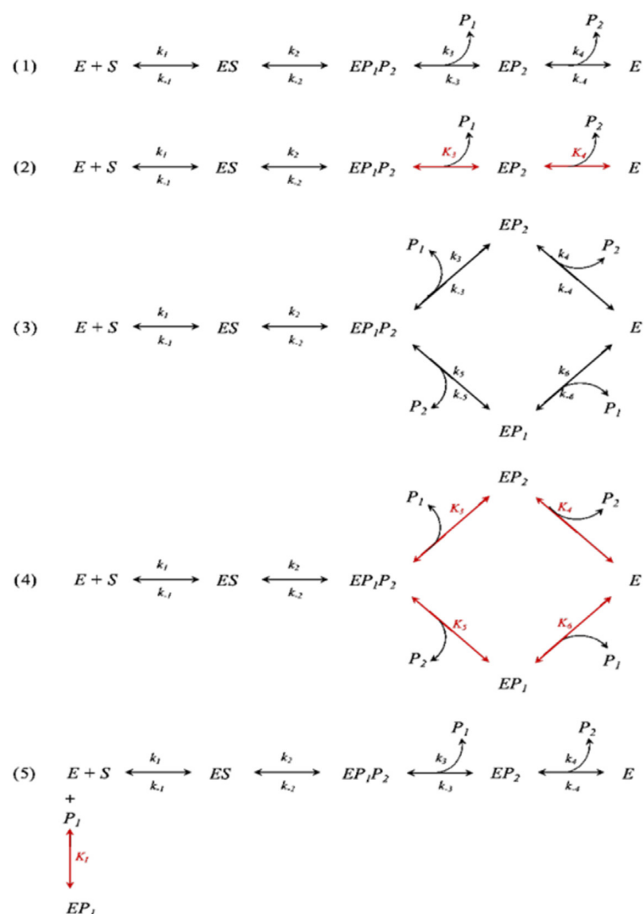The free energy profiles were constructed using the Jarzynski equality [20] (Equation 2)

$$\Delta F = -\frac{1}{\beta}\langle e^{-\beta W}\rangle \tag{2}$$

where $\beta = 1/k_\beta T$ and $W$ is the irreversible work performed. For each SMD trajectory, the work was computed by integrating the external force $f$ over time. The Fluctuation-Dissipation estimator of the free energy $\widehat{F}_{FD} = \overline{W} - \frac{1}{2}\beta\sigma_W^2$, was used to construct free energy profiles after verifying that the work distribution was Gaussian in each case [21].

## RESULTS

### Schemes for product release mechanisms in enzyme reactions

In order to determine the kinetic mechanism of product release after hydrolysis of ATP by NS3h, we considered the following five kinetic schemes:

**Figure 2.** Inhibition of ATPase activity ($v_i$) by phosphate (Pi). Symbols indicate values of ATPase activity at: (●) 8, (●) 4, (●) 1 and (●) 0.25 mM ATP in the presence of Pi concentrations indicated on the abscissa. Continuous lines are the plot of mathematical expression of scheme 1 (Equation 3) with parameter values shown in Table 2. Line thickness corresponds to the ATP concentration, with thicker lines representing higher concentrations. Experiments were performed in 'working buffer' at 25°C, pH 6.5 and enough KCl, NaCl and MgCl$_2$ to obtain the following final ionic concentrations ($I = 0.1395$ M): 130 mM K$^+$, 60 mM Na$^+$ and 1.5 mM free Mg$^{2+}$.
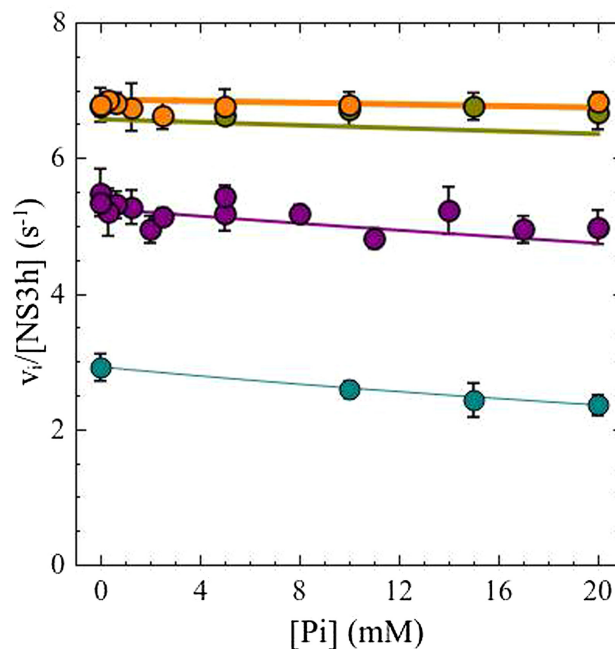
Together, these schemes consider key aspects of the product release mechanism, namely: (a) whether the products are released randomly or in an ordered sequence; (b) which of the products is released first in the case of an ordered mechanism and (c) whether the product release steps are in rapid equilibrium.

We first verified that the steady-state rate equations of these schemes in the presence of products are distinguishable from each other (detailed deduction of the rate equation of each scheme is provided in SI). Then, in order to determine which of the five schemes most accurately describes the mechanism of product release in NS3h, we conducted product-inhibition studies by measuring steady-state ATPase activity in the presence of varying initial concentrations of ADP and/or Pi. To do this, we used [γ-$^{32}$P] labelled ATP as a tracer of substrate and quantified the [$^{32}$P]Pi released after the hydrolysis of the nucleotide (see Materials and Methods).

**ATPase activity of NS3h in the presence of products**

Since both Pi and ADP were added to the reaction medium as sodium and/or potassium salts, increases in their concentrations are concomitant with that of the cations and with the ionic strength. Therefore, to maintain the same ionic strength in all experimental conditions despite the wide variation of Pi and ADP concentrations, it was necessary to initially fix a working reaction media with relatively high ionic strength and balance the sodium and/or potassium present due to the ADP and/or the Pi by ad-

justing the amount of NaCl and KCl added to the amount needed to reach the final concentration of ions in the reaction medium.

Figure 2 shows the change in ATPase activity of NS3h with increasing initial concentrations of Pi. Experiments were repeated for four different ATP concentrations (colored series, Figure 2).

The maximum initial Pi concentration (20 mM) was chosen as to not interfere with the quantitative extraction of labeled phosphate from the organic phase (see SI Supplementary Figure S1). Figure 2 shows that Pi exerts a slight inhibitory effect, which becomes more pronounced as the ATP concentration decreases.

Similarly, Figure 3 shows the change in ATPase activity of NS3h with increasing initial concentrations of ADP. Once more, these experiments were repeated for different initial ATP concentrations, in both absence and presence of Pi. The inhibitory effect of ADP on the ATPase activity of NS3h was observed for the entire range of ATP concentrations considered (0.05–4 mM), regardless of the addition of Pi (10 or 20 mM). It should be noted that the ADP used in these experiments contains a trace amount (5%) of free phosphate. Therefore, all experiments performed in the presence of ADP necessarily also contained phosphate. However, the contribution of the contaminant to the inhibitory effect on ATPase activity is practically negligible given that NS3h has a very low affinity for phosphate (see
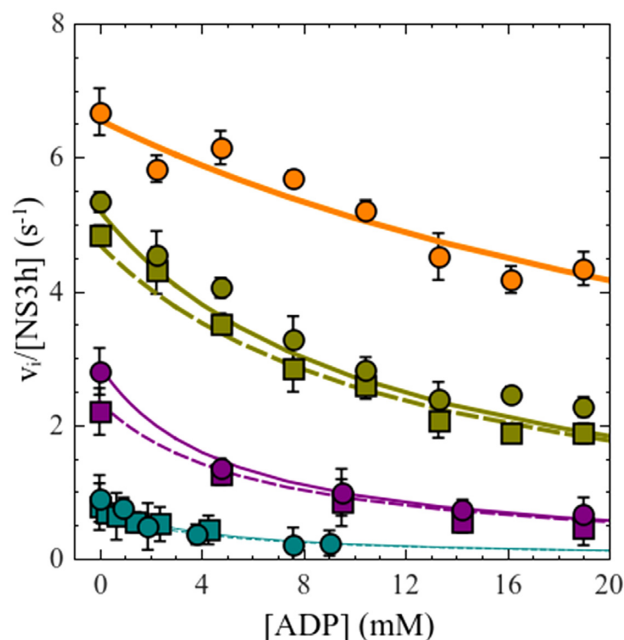
**Figure 3.** Inhibition of ATPase activity ($v_i$) by ADP. Symbols indicate ATPase activity values at: (●) 4, (●) 1, (●) 0.25, (●) 0.05 mM ATP; (■) 1 and (■) 0.25 mM ATP in the presence of 20 mM of Pi and, (■) 0.05 mM of ATP in the presence of 10 mM Pi at ADP concentrations indicated on the abscissa. The ATPase activity values obtained in the absence or presence of Pi are represented with circles or squares respectively. Lines are the plot of mathematical expression of scheme 1 (Equation 3) with parameter values shown in Table 1. The solid lines correspond to the experiments carried out in the absence of Pi and the dashed lines to those carried out in the presence of Pi. Line thickness corresponds to the ATP concentration, with thicker lines representing higher concentrations. Experiments were performed in 'working buffer' at 25°C, pH 6.5 and enough KCl, NaCl and MgCl$_2$ to obtain the following final ionic concentrations ($I = 0.1395$ M): 130 mM K$^+$, 60 mM Na$^+$ and 1.5 mM free Mg$^{2+}$.

**Figure 4.** Inhibition of ATPase activity in the presence of ADP, Pi or ADP + Pi mixtures. Symbols indicate ATPase activity values at: (●) 0 (control), (■) 20 mM Pi, (◆) 2 mM ADP, (▲) 2 mM ADP + 5 mM Pi, (◆) 10 mM ADP and (▲) 12 mM ADP + 20 mM Pi. The ATPase activity values obtained in the absence of products are represented with circles, with squares in presence of Pi, with diamonds in presence of ADP and with triangles a combination of both products. Lines are the plot of mathematical expression of scheme 1 (Equation 3) with parameter values shown in Table 2. The solid line corresponds to the experiments performed in absence of products. The dashed lines correspond to the experiments carried out in the presence of ADP, dotted lines in the presence of Pi, and discontinuous line a combination of ADP and P$_i$. Experiments were performed in 'working buffer' at 25°C, pH 6.5 and enough KCl, NaCl and MgCl$_2$ to obtain the following final ionic concentrations ($I = 0.1395$ M): 130 mM K$^+$, 60 mM Na$^+$ and 1.5 mM free Mg$^{2+}$.
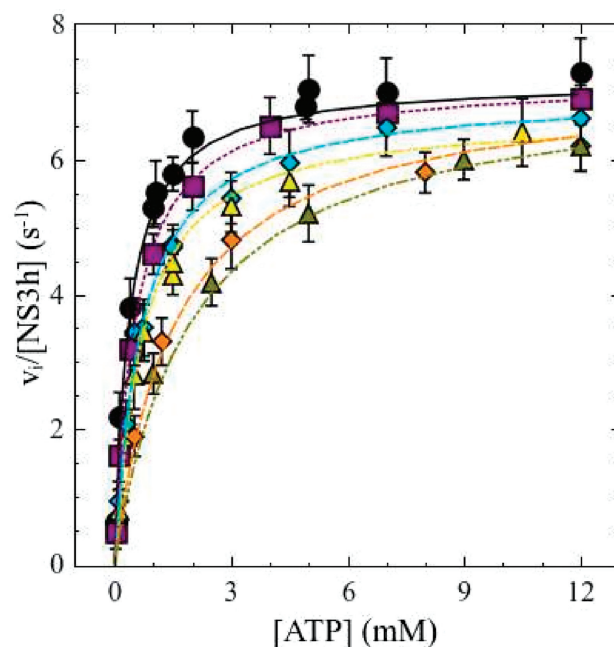
Figure 2). Even so, the trace amounts of Pi present in ADP solutions were accounted for in all calculations, simulations and equation fitting.

Finally, Figure 4 shows the inhibitory effect of ADP, Pi and ADP + Pi mixtures on the ATPase activity of NS3h.

## Assignment of product release model

The set of experimental results shown in Figures 2–4 was used to establish which of the models (schemes 1–5), if any, best describes the kinetic mechanism of product release in NS3h. To do so, we first fit, with the appropriate thermodynamic constraints, each of the Equations (1), (4), (7), (10) and (13) in SI to all experimental data simultaneously using nonlinear regression analysis and then we evaluated the performance of each model.

During the fitting procedure, we utilized the Haldane relationship as a thermodynamic constraint. For each steady-state rate equation there is at least one relationship of this type between the kinetic parameters and the equilibrium constant. For example, if we rewrite the rate equation of scheme 1 (Equation 3) using Cleland's nomenclature (22) the new parameters of the numerator and denominator can be expressed in more meaningful terms, namely the Michaelis constants and inhibition constants, which are de-

fined for each reactant ($K_{M,x}$ and $K_{i,x}$, respectively), in addition to the maximum velocities in the forward and reverse directions ($V_1$ and $V_2$, respectively), such that the relation with the $N_i$ and $D_i$ coefficients of Equation (3) becomes:

$$V_1 = \left(\frac{N_1}{D_1}\right) \quad V_2 = \left(\frac{N_2}{D_5}\right) \quad K_{M,ATP} = \left(\frac{D_0}{D_1}\right)$$

$$K_{M,Pi} = \left(\frac{D_3}{D_5}\right) \quad K_{M,ADP} = \left(\frac{D_2}{D_5}\right)$$

$$K_{i,ATP} = \left(\frac{D_2}{D_4}\right) \quad K_{i,Pi} = \left(\frac{D_1}{D_4}\right)$$

$$K_{i,ADP} = \left(\frac{D_0}{D_3}\right)$$

where these kinetic parameters are not independent of each other, rather they are related to the equilibrium constant through the Haldane relationship:

$$K_{eq} = \frac{V_1 K_{i,Pi} K_{M,ADP}}{V_2 K_{i,ATP}} = \frac{V_1 K_{M,Pi} K_{i,ADP}}{V_2 K_{M,ATP}}$$

**Table 1.** AIC values

| Scheme | First: Pi, second: ADP | | First: ADP, second: Pi |
| --- | --- | --- | --- |
| 1 | − 364.84 | | − 101.24 |
| 2 | − 335.5 | | − 30.22 |
| 3 | | 275.05 | |
| 4 | | − 21.72 | |
| 5 | −362.8 | | − 101.08 |

Akaike information criterion (AIC) values for the fitting of rate equations of schemes 1–5 (Equations (1), (4), (7), (10) and (13) in S.I.) to all experimental data simultaneously. The AIC was calculated as follows: $AIC_C = n.ln[S(\theta)_{min}/n] + 2.(p + 1)(n/n - p - 2)$, where $S(\theta)_{min}$ is the minimum residual sum of square between the observed and predicted values; $n$ is the number of data points and $p$ is the number of parameters. The best model corresponds to that with the minimum AIC value.

Analogous relationships were found for each of the five kinetic schemes and were used as thermodynamic constraints.

The value of the equilibrium constant of ATP hydrolysis in the corresponding experimental conditions (pH 6.5, $T = 25°C$, ionic strength = 0.2 and $[Mg^{2+}] = 1$ mM) was taken from the literature, $7.17 \times 10^7$ mM (23), and was used as a thermodynamic constraint (to within one order of magnitude) during the fitting procedure.

The equations corresponding to the different kinetic models differ in the number of parameters they each have, which compromises a fair comparison of their goodness of fit. Therefore, to evaluate the performance of each model, we used the AIC, which not only takes into account the goodness of fit, but also includes a penalty that is an increasing function of the number of estimated parameters. Given a set of models to represent the data, we identified the preferred model as the one with the minimum AIC value.

Table 1 presents the AIC values from the fittings of the rate equations corresponding to schemes 1-5 (see Equations 1, 4, 7 and 10 in SI) to all experimental data (Figures 2–4). Except for the case of random product release, each equation was tested with both possible orders of product release, i.e. Pi released followed by ADP, and vice versa. The AIC values in Table 1 range from approximately −365 to 275. Two models, corresponding to kinetic schemes (1) and (5), both with Pi as the first product released, have the lowest AIC values, which are nearly equivalent (−364.84 and -362.8, for schemes 1 and 5, respectively). We note that kinetic scheme (5) only adds one step to scheme (1) to contemplate the possibility that the first product released may be a competitive inhibitor as well as a mixed inhibitor of the enzyme. Nevertheless this extension of the scheme, which incorporates an additional parameter to the steady-state rate equation with respect to that of scheme (1), does not improve the fit of the AIC score.

Thus, according to the criteria of model selection, scheme 1 with Pi as the first product released followed by ADP is the model that best represents the kinetic behavior of product release in the catalytic cycle of NS3h. The rate equation corresponding to this model is shown in Equation (3) (see SI for detailed deduction):

$$\frac{v}{[E_T]} = \frac{N_1[S] - N_2[P_1][P_2]}{D_0 + D_1[S] + D_2[P_1] + D_3[P_2] + D_4[S][P_1] + D_5[P_1][P_2]} \quad (3)$$

Table 2 shows the best-fit parameter values of the ordered sequential mechanism of product release, with Pi as the first product released and ADP the second. Continuous lines in Figures (2) to (4) are the plot of Equation (3) with parameter values from Table 2 obtained by simultaneous fitting to all experimental data using nonlinear regression analysis.

**Novel open-loop conformation facilitates Pi release**

To evaluate the proposed sequential mechanism, we constructed free energy profiles (FEPs) for each of the possible initial steps, i.e. ADP or Pi release, using multiple SMD simulations. During each SMD simulation, a time-dependent harmonic potential was introduced to gradually pull either ADP or Pi out of the active site along a predefined vector.

As mentioned in the introduction, our previous results (12) highlight a novel open-loop conformation of the β6−β1′ loop, which could serve as an exit route for Pi, however this open-loop conformation was only sampled in approximately 10% of 1.2 microseconds of MD simulations, such that the most probable conformation of the product-bound state coincides with the crystallographic (closed-loop) structure. With this in mind, we first evaluated both possible initial steps of product release exclusively via the canonical channel, with the protein in its closed-loop conformation (Figure 5A and B). ADP release via the canonical channel has a $\Delta G_{dissoc}$ value and barrier height ($\Delta G^{\ddagger}$) of approximately 50 and 55 kcal/mol, respectively. Similarly, Pi release via the canonical channel is also highly endergonic with a $\Delta G_{dissoc}$ value and $\Delta G^{\ddagger}$ of 30 and 40 kcal/mol, respectively.

We then considered the novel open-loop conformation and evaluated the release of ADP via the canonical and Pi via the backdoor channels (Figure 5C and D). We note that ADP release via the backdoor channel was not considered as the channel is too narrow for this process. These FEPs show that ADP release via the canonical channel is affected by the opening of the β6−β1′ loop, as the $\Delta G_{dissoc}$ becomes approximately null, in contrast to the 50 kcal/mol in the case of the closed loop conformation, though the resulting free energy barrier is still high (approximately 40 kcal/mol, Figure 5C). In contrast, the release of Pi via the backdoor channel is slightly exergonic, with $\Delta G_{dissoc}$ of nearly -10 kcal/mol, and is clearly the kinetically favored first step, with a barrier of approximately 20 kcal/mol (Figure 5D).

To further validate this proposed sequentiality of Pi release followed by ADP release, we considered the subsequent step of ADP release. To construct the FEP for this step, we performed classical MD simulations of the post-Pi-release state obtained from the SMD simulations corresponding to Supplementary Figure S6 SI, after first removing the Pi molecule from the system, followed by SMD simulations to evaluate ADP release. The resulting FEP (Figure 6) indicates that the subsequent release of ADP is slightly exergonic with a barrier height (approximately 25 kcal/mol) comparable to that of initial Pi release. We highlight that this FEP corresponds to ADP release through the canonical channel in the open-loop conforma-

**Table 2.** Best-fitting values and standard errors of the parameters of the ordered sequential mechanism of product release with $P_i$ as the first product released and ADP the second

| Cleand's parameter | Value | Units | Parameter of Equation (3) | Value | Units |
|---|---|---|---|---|---|
| $V_1/[E]_T$ | $7.18 \pm 0.07$ | s$^{-1}$ | $N_1/D_1$ | $7.18 \pm 0.07$ | s$^{-1}$ |
| $V_2/[E]_T$ | $0.006 \pm 0.001$ | s$^{-1}$ | $N_2/D_1$ | $(3.75 \pm 0.02) \times 10^{-7}$ | mM$^{-1}$s$^{-1}$ |
| $K_{M, ATP}$ | $0.367 \pm 0.019$ | mM | $D_0/D_1$ | $0.367 \pm 0.019$ | mM |
| $K_{M, Pi}$ | $(2.0 \pm 1.4) \times 10^3$ | mM | $D_1/D_1$ | 1 | dimensionless |
| $K_{M, ADP}$ | $(1.19 \pm 0.36) \times 10^2$ | mM | $D_2/D_1$ | $0.0045 \pm 0.0016$ | dimensionless |
| $K_{i, ATP}$ | $43 \pm 24$ | mM | $D_3/D_1$ | $0.126 \pm 0.007$ | dimensionless |
| $K_{i, Pi}$ | $(5.8 \pm 3.2) \times 10^3$ | mM | $D_4/D_1$ | $(1.73 \pm 0.97) \times 10^{-4}$ | mM$^{-1}$ |
| $K_{i, ADP}$ | $2.9 \pm 0.3$ | mM | $D_5/D_1$ | $(6.25 \pm 0.87) \times 10^{-5}$ | mM$^{-1}$ |
| $K_{eq}$ | $(1.91 \pm 0.26) \times 10^7$ | mM | | | |

These values were obtained using simultaneous fitting to all experimental results (Figures 2–4) by nonlinear regression analysis. The value of $K_{eq} = 7.17 \times 10^7$ mM, within one order of magnitude, was used as a thermodynamic constraint during the fitting process.

To fit Equation (3) to the experimental data it should be reparametrized (dividing by $D_1$) in order to overcome the indeterminacy of the original parameters:

$$\frac{v}{[E_T]} = \frac{\frac{(N_1/D_1)[S]}{1+(D_4/D_1)[P_1]} - \frac{(N_2/D_1)[P_1][P_2]}{1+(D_4/D_1)[P_1]}}{[S] + \frac{(D_0/D_1)+(D_2/D_1)[P_1]+(D_3/D_1)[P_2]+(D_5/D_1)[P_1][P_2]}{1+(D_4/D_1)[P_1]}}$$

tion. Though we attempted to construct the corresponding FEP for the closed-loop conformation, the ADP-Mn$^{2+}$ complex did not effectively dissociate from the protein in this case (see Supplementary Figure S7 SI).

### Effect of RNA on product release mechanism

Because the NTPase activity of NS3h is known to be stimulated by RNA, we sought to evaluate the impact that RNA has specifically on the product release mechanism. We constructed FEPs corresponding to initial ADP (via the canonical channel) and Pi release (via the backdoor channel) after removal of the bound ssRNA segment, but specifically preserving the open-loop conformation (Figure 7). In contrast to ADP release in the presence of RNA (Figure 5C; $\Delta G_{dissoc} \sim 0$ kcal/mol and $\Delta G^{\ddagger} \sim 40$ kcal/mol), the FEP for ADP release in the absence of RNA was highly endergonic (Figure 7 A; $\Delta G_{dissoc} \sim 50$ kcal/mol and $\Delta G^{\ddagger} \sim 55$ kcal/mol). Despite the preserved open conformation of the β6−β1′ loop, the FEP in the absence of RNA reflects similar values to those observed in the case of the closed loop conformation in presence of RNA (Figure 5A; $\Delta G_{dissoc} \sim 50$ kcal/mol and $\Delta G^{\ddagger} \sim 55$ kcal/mol). The Pi release step via the backdoor channel, in constrast, is similarly exergonic both in presence and absence of RNA (Figure 7 B), with comparable barrier heights ($\sim 20$ kcal/mol) and $\Delta G_{dissoc}$ values (between –20 and –10 kcal/mol). Together these results suggest that Pi release, specifically via the backdoor channel, likely precedes ADP relase, regardless of the presence of RNA. Furthermore, the conformation of the β6−β1′ loop and the presence of RNA both appear to impact the release of ADP (see Discussion).

### Molecular characterization of product release pathways

A closer analysis of the 500 SMD trajectories used to construct the FEPs in Figures 5 and 7 provide insight into the atomistic details of the product release mechanism. The free energy barrier of approximately 20 kcal/mol observed in the FEP of the release of Pi via the backdoor channel (Figure 5D) corresponds to rearrangements in the first coordination sphere of the bound Mn$^{2+}$ ion; the onset of the free energy barrier coincides with Pi being pulled out of the initial coordination sphere (Supplementary Figure S5 SI), and the free energy lowers when a third water molecule is incorporated into the first coordination sphere. This cost of reorganization of the initial coordination sphere contributes to the free energy barrier in each case, more so for ADP, which occupies two coordination sites initially.

## DISCUSSION

In the present work, we proposed a systematic procedure of product-inhibition studies to establish the order of product release in the catalytic cycle of ATP hydrolysis by the DENV NS3 helicase. The procedure consists in testing five kinetic models, each one corresponding to one of the general mechanisms of product release for uni-bi enzymatic reactions, in their ability to fit (or describe) the experimental data.

We first showed that the steady-state rate equations derived for each scheme in the presence of products are kinetically distinguishable from one another. In this way, by performing steady-state ATPase activity assays we would be able to determine whether products are randomly released or in a fixed order; in the case of the latter, which of the products is first released and whether the product release steps are in rapid equilibrium. We highlight that the theoretical-experimental procedure presented here is of general application and can be used for the same study in any NTPase.

Based on steady-state ATPase experiments in the presence of different initial concentrations of ADP and Pi, and with the imposition of the Haldane equation as a thermodynamic constraints in the fitting procedure, and through the use of the AIC for model selection, we concluded the following: the pathway of the catalytic cycle of ATP hydrolysis by NS3h proceeds through an apparent Uni-Bi ordered sequential mechanism that includes a ternary complex intermediate (NS3h-Pi-ADP) that evolves releasing the first product, Pi, and subsequently ADP.

Table 1 shows the values of the AIC obtained by fitting the parameters of each kinetic scheme to the data. All of the schemes corresponding to ordered mechanisms of product
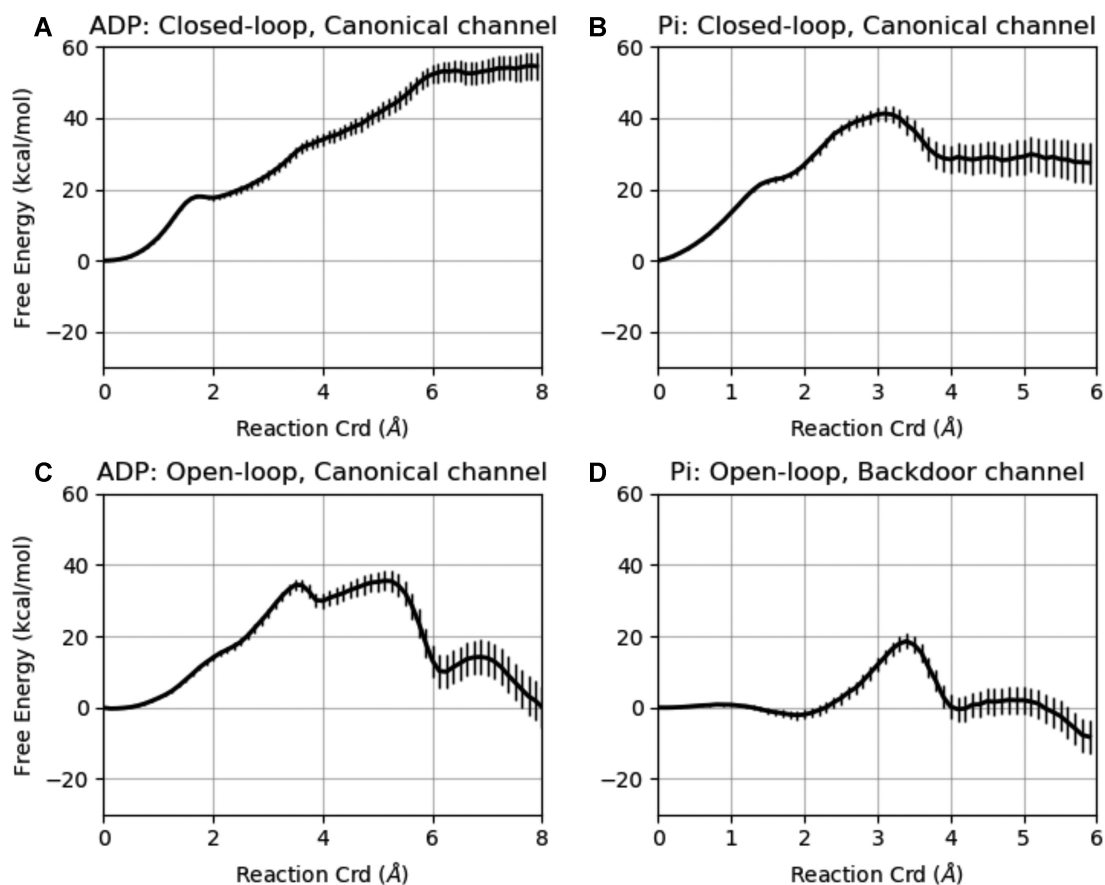
**Figure 5.** Free energy profiles for initial release of either ADP or Pi from product-bound state. Release of (**A**) ADP or (**B**) Pi via the canonical channel, with initial structures in the closed-loop conformation are shown on the top panel; release of (**C**) ADP via the canonical channel, and (**D**) Pi via the backdoor channel, with initial structures in the open-loop conformation are shown on the bottom panel. In all cases, a 7-base ssRNA segment was bound to the protein.
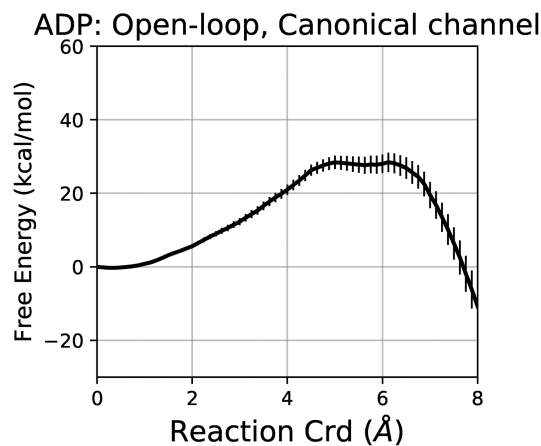


**Figure 6.** Free energy profile for ADP-$Mn^{2+}$ release via the canonical channel after initial $P_i$ release in presence of a 7-base ssRNA segment.

release fit better than those corresponding to random mechanisms. This result was not altogether surprising, since, to our knowledge, no sequential random mechanism of product release has ever been reported for any ATPase. The AIC values also show, and in this sense provide strong evidence, that the best performance of each ordered mechanism always corresponds to the same order of product release: Pi followed by ADP.

**Selection of kinetic model**

On examining Table 1, we can also see that, on the one hand, product release steps of the catalytic cycle of NS3h are not in rapid equilibrium, as the AIC value for scheme 2 ($-335.5$) is greater than those of schemes 1 ($-364.84$) and 5 ($-362.8$). On the other hand, our experimental results do not allow us to distinguish whether or not Pi competes with ATP for the catalytic site of the enzyme, as the AIC values for schemes 1 and 5 are quite close.

We cannot rule out that this lack of sensitivity may be due to the difficulty in reaching a larger percent inhibition of ATPase activity by Pi and ADP (20 and 60%, respectively). The maximum inhibition reached was conditioned by the highest concentrations of ADP and Pi that we could work with (20 mM in both cases). Greater concentrations of ADP would affect the constancy of ionic strength of the medium—commercial ADP contains 7% sodium—that up to 20 mM is adjusted by the addition of salts, and greater concentrations of Pi would interfere with the extraction of [$^{32}$P]Pi (see SI).
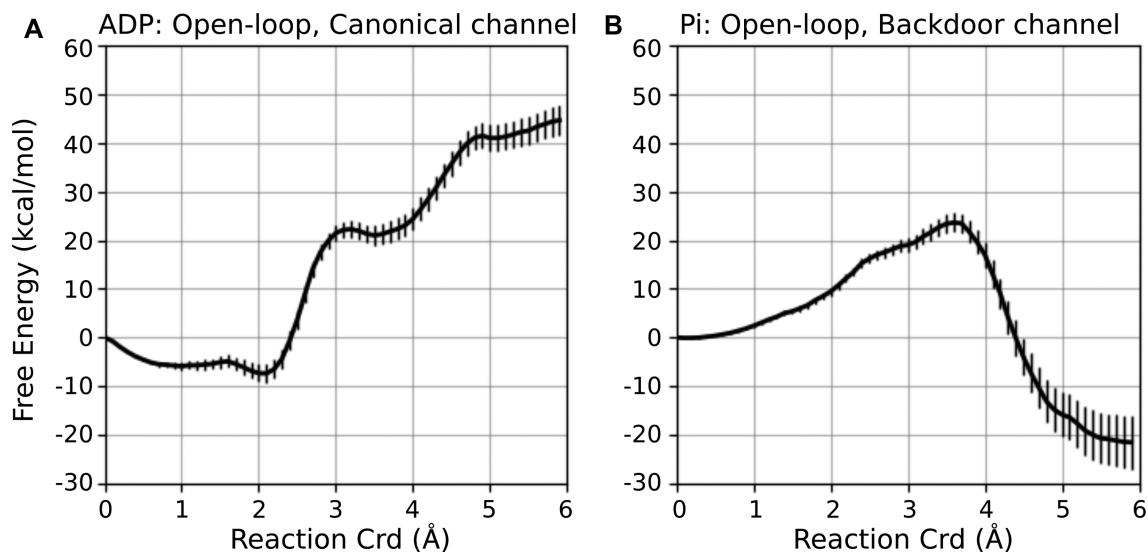
**Figure 7.** Effect of RNA on product-release free energy profiles. FEPs for initial release of (**A**) ADP via the canonical channel or (**B**) P$_i$ via the backdoor channel, with initial structures in the open-loop conformation are shown. In both cases, ssRNA was removed from the respective conformations and the system was allowed to equilibrate before generating the initial configurations for SMD simulations (see Methods).

**Fitted model parameters**

The fitted values of the Michaelis constants ($K_{M, ATP}$, $K_{M, Pi}$ and $K_{M, ADP}$) show that the DENV NS3h is much more sensitive to the capacity of ATP to modulate its ATPase activity than it is to that of either ADP or Pi . The inhibitory effects of the products Pi and ADP on the ATPase activity is reflected in the magnitudes of the inhibition constants ($K_{i, Pi}$ = 5.77 x 10$^3$ mM and $K_{i, ADP}$ = 2.9 mM). We note that, for scheme 1, $K_{i, ADP}$ is a true substrate-dissociation constant whereas $K_{i, Pi}$ is not (expressions in terms of the kinetic rate constants can be found in Supplementary Information).

In this study, the Haldane relationship was implemented to restrict the number of kinetic mechanisms and ensure the thermodynamic consistency of the models. In addition, from this implementation the value of $K_{eq}$ for the ATP hydrolysis was also obtained. It is worth noting that although rate data are inherently less accurate than equilibrium measurements and evaluation of $K_{eq}$ from the ratio of composite kinetic parameters is fraught with error, the estimation of $K_{eq}$ resulting from the fitting of kinetic scheme (1) to the experimental data ($K_{eq}$ = 1.91 x 10$^7$ mM, Table 2) is acceptably close to the literature value (23).

**Mechanistic relevance of the novel open-loop conformation**

Based on the crystallographic conformation of the NS3h–RNA–ADP–Pi–Mn$^{2+}$ complex, we used steered molecular dynamics simulations to construct free energy profiles for the initial release of Pi and ADP from the nucleotide binding cleft (canonical channel). A comparison of these FEPs suggests that, in agreement with experimental results, the initial release of Pi is more favorable than that of ADP, albeit with a substantial barrier height of 40 kcal/mol. If we further consider that the initial release of Pi can occur through the novel backdoor channel of the open-loop conformation observed in previous simulations (12), this initial

release of Pi is more favorable still, with a barrier height of approximately 20 kcal/mol.

The finding that the backdoor channel is the kinetically favored route for the release of Pi during the catalytic cycle of ATP hydrolysis is further supported by an independent experimental observation. The difference between the computationally estimated rate constants for Pi release via the canonical channel (approx. 5 × 10$^{-17}$ s$^{-1}$) and the backdoor channel (approx. 0.02 s$^{-1}$) reflects the radical difference in the kinetics of Pi release via the two routes, even with the large uncertainty of $\pm$ 3 orders of magnitude (corresponding to ±4 kcal/mol in the FEPs) observed in the estimated rate constants. Considering, furthermore, that all first-order rate constants of the catalytic cycle in the forward direction must be equal to or greater than the measured turnover number of the ATPase activity, which is 7.18 $\pm$ 0.07 s$^{-1}$ (Table 2), the computationally estimated rate constants would effectively rule out the possibility that Pi release occurs via the canonical channel in the closed-loop crystallographic conformation of the DENV NS3h.

When we further consider the subsequent step of ADP release through the canonical channel, the open-loop conformation again appears to play an important role. Despite our efforts to guide the release of ADP with the NS3h in the closed loop conformation, the corresponding work values were larger than those of any other scenario explored and the ADP-Mn$^{2+}$ complex did not effectively dissociate from the protein (Supplementary Figure S7 SI). In contrast, when we evaluated the same process of ADP release post Pi release, but in the open-loop conformation, we found it to be exergonic with a low barrier height comparable to that of initial Pi release via the backdoor channel (Figure 6). Together these results not only validate the sequentiality of Pi release followed by ADP release, but also provide new insight into the relevance of the open-loop conformation of the DENV NS3h in both product release steps.

Similar back-door pathways and the importance of a hinge/linker loop have been proposed for Pi release in other motor proteins (24–26), and in the case of the extensively studied myosins, such a back-door mechanism is widely accepted (24,25). In this context, the release of Pi has also been reported to precede that of ADP (27), and there is a general consensus that Pi release via the back door is the precursor to the power stroke in myosins (25).

The importance of the open-loop conformation in the product release mechanism of the NS3 helicase, and the conservation of this loop among other NS3 helicases of the Flaviviridae family, make it an interesting conformation to consider in future drug discovery efforts. Allosteric inhibitors of the NS3h that leverage this conformation could serve as novel antiviral therapeutics (28).

We note that the NS3h protein used in the *in vitro* assays corresponds to DENV serotype 2, whereas the simulated model corresponds to serotype 4. Though the conclusion that the release of Pi precedes that of ADP was drawn independently from both the computational and experimental results, the specific insight into the separate pathways for Pi and ADP release was derived from the computational results. We cannot discard the possibility that the role of the open-loop conformation described here is unique to the NS3h of DENV serotype 4; however, given the 82 % sequence identity of the NS3h of the two serotypes, in particular including the TAT sequence of Motif III on the β6−β1′ loop, as well as their reported comparable ATPase activity in solution (29), we would consider this possibility to be unlikely. On the contrary, we envision that the role of the open-loop conformation is likely shared with other viral NS3h proteins as well.

### Impact of RNA on product release mechanism

Because the ATPase activity of the DENV NS3h is enhanced 7-8-fold in the presence of RNA (5), we also asked the question of whether the presence of bound RNA may specifically impact the order of product release. If we consider this enhancement in rate constant in terms of barrier height ($<1$ kcal/mol difference), we highlight that it is smaller than the uncertainty of the barrier heights of the FEPs for Pi release. In this way, it is encouraging that the barrier heights for Pi release with and without RNA are within error of each other, further indicating consistency between the computational model that contemplates the open-loop conformation and the experimental results.

### Pi release and coupling of ATPase and helicase activities

In our previous work, we observed that the opening of the β6−β1′ loop was preceded by a separation of the RNA-binding residues on subdomains 1 and 2, and was followed by a separation of nucleotide-binding residues in the catalytic site. We highlight that Motif III, a conserved helicase sequence motif, is located precisely at the start of the β6−β1′ loop, and appears to be key in regulating the loop conformation.

In particular, Thr 317 of Motif III interacts with Gln 456 in the catalytic site, an interaction that correlates with the alternating flexible-rigid structural states during ATP hydrolysis. That is, the Thr 317-Gln 456 interaction is nearly always observed in the rigid closed-loop ATP-bound conformation, whereas it is more labile in the flexible free and product-bound states, with the interaction necessarily broken in the open loop conformation. Interestingly, the single mutation of this conserved Thr residue to Ala in other RNA helicases has resulted in an uncoupling of helicase and ATPase activities in the NPH-II RNA helicase of the Vaccinia virus (30). Motif III has also been implicated in linking RNA binding to ATPase activities in the Yeast DEAD-Box Protein Ded1 (31).

Here we have further demonstrated that Pi release is promoted by the open-loop conformation, and that it precedes ADP release. The sequentiality of Pi release followed by ADP, as well as Pi release driving the power stroke seem to be characteristics of the working cycles of RecA and related ATPase motors (32). One hypothesis that stems from our results is that the conformational change involving the β6−β1′ loop that promotes Pi release is implicated in the transduction process that couples the catalytic cycle of hydrolysis of NTP to the mechanical cycle at the RNA binding site. The role of the β6−β1′ loop is likely generalizable to other NS3 helicases. We further hypothesize that both processes (the conformational change of the β6−β1′ loop and Pi release) are the precursors of the displacement step, whether by a power stroke, thermal diffusion or some combination of these two limiting regimes, underlying the translocation and RNA unwinding activities of NS3h.

## DATA AVAILABILITY

All data presented in this manuscript can be made available upon request to the corresponding authors.

## SUPPLEMENTARY DATA

Supplementary Data are available at NAR Online.

## REFERENCES

1. Matusan,A.E., Pryor,M.J., Davidson,A.D. and Wright,P.J. (2001) Mutagenesis of the dengue virus type 2 NS3 protein within and outside helicase motifs: effects on enzyme activity and virus replication. *J. Virol.*, **75**, 9633–9643.

2. Heaton,N.S., Perera,R., Berger,K.L., Khadka,S., Lacount,D.J., Kuhn,R.J. and Randall,G. (2010) Dengue virus nonstructural protein 3 redistributes fatty acid synthase to sites of viral replication and increases cellular fatty acid synthesis. *Proc. Natl. Acad. Sci. U.S.A.*, **107**, 17345–17350.

3. Perera,R. and Kuhn,R.J. (2008) Structural proteomics of dengue virus. *Curr. Opin. Microbiol.*, **11**, 369–377.

4. Li,H., Clum,S., You,S., Ebner,K.E. and Padmanabhan,R. (1999) The serine protease and RNA-stimulated nucleoside triphosphatase and RNA helicase functional domains of dengue virus type 2 NS3 converge within a region of 20 amino acids. *J. Virol.*, **73**, 3108–3116.

5. Incicco,J.J., Gebhard,L.G., González-Lebrero,R.M., Gamarnik,A.V. and Kaufman,S.B. (2013) Steady-state NTPase activity of Dengue virus NS3: number of catalytic sites, nucleotide specificity and activation by ssRNA. *PLoS One*, **8**, e58508.

6. Gebhard,L.G., Kaufman,S.B. and Gamarnik,A.V. (2012) Novel ATP-independent RNA annealing activity of the dengue virus NS3 helicase. *PLoS One*, **7**, e36244.

7. Benarroch,D., Selisko,B., Locatelli,G.A., Maga,G., Romette,J.-L. and Canard,B. (2004) The RNA helicase, nucleotide 5′-triphosphatase, and RNA 5′-triphosphatase activities of Dengue virus protein NS3 are $Mg^{2+}$-dependent and require a functional Walker B motif in the helicase catalytic core. *Virology*, **328**, 208–218.

8. Chernov,A.V., Shiryaev,S.A., Aleshin,A.E., Ratnikov,B.I., Smith,J.W., Liddington,R.C. and Strongin,A.Y. (2008) The two-component NS2B-NS3 proteinase represses DNA unwinding activity of the West Nile virus NS3 helicase. *J. Biol. Chem.*, **283**, 17270–17278.

9. Pang,P.S., Jankowsky,E., Planet,P.J. and Pyle,A.M. (2002) The hepatitis C viral NS3 protein is a processive DNA helicase with cofactor enhanced RNA unwinding. *EMBO J.*, **21**, 1168–1176.

10. Jankowsky,E., Gross,C.H., Shuman,S. and Pyle,A.M. (2000) The DExH protein NPH-II is a processive and directional motor for unwinding RNA. *Nature*, **403**, 447–451.

11. Luo,D., Xu,T., Watson,R.P., Scherer-Becker,D., Sampath,A., Jahnke,W., Yeong,S.S., Wang,C.H., Lim,S.P., Strongin,A. *et al.* (2008) Insights into RNA unwinding and ATP hydrolysis by the flavivirus NS3 protein. *EMBO J.*, **27**, 3209–3219.

12. Sarto,C., Kaufman,S., Estrin,D. and Arrar,M. (2020) Nucleotide-dependent dynamics of dengue NS3 helicase. *Biochim. Biophys. Acta Proteins Proteom.*, **1868**, 140441.

13. Cavaluzzi,M.J. and Borer,P.N. (2004) Revised UV extinction coefficients for nucleoside-5′-monophosphates and unpaired DNA and RNA. *Nucleic Acids Res.*, **32**, e13.

14. Smith,R.M., Martell,A.E. and Chen,Y. (1991) Critical evaluation of stability constants for nucleotide complexes with protons and metal ions and the accompanying enthalpy changes. *Pure Appl. Chem.*, **63**, 1015–1080.

15. Kinney,R.M., Butrapet,S., Chang,G.J., Tsuchiya,K.R., Roehrig,J.T., Bhamarapravati,N. and Gubler,D.J. (1997) Construction of infectious cDNA clones for dengue 2 virus: strain 16681 and its attenuated vaccine derivative, strain PDK-53. *Virology*, **230**, 300–308.

16. Pace,C.N., Vajdos,F., Fee,L., Grimsley,G. and Gray,T. (1995) How to measure and predict the molar absorption coefficient of a protein. *Protein Sci.*, **230**, 2411–2423.

17. Schwarzbaum,P.J., Kaufman,S.B., Rossi,R.C. and Garrahan,P.J. (1995) An unexpected effect of ATP on the ratio between activity and phosphoenzyme level of $Na^+/K^+$-ATPase in steady state. *Biochim. Biophys.*, **1233**, 33–40.

18. Yamaoka,K., Nakagawa,T. and Uno,T. (1978) Application of Akaike's information criterion (AIC) in the evaluation of linear pharmacokinetic equations. *J. Pharmacokinet. Biopharm.*, **6**, 165–175.

19. Phillips,J.C., Braun,R., Wang,W., Gumbart,J., Tajkhorshid,E., Villa,E., Chipot,C., Skeel,R.D., Kalé,L. and Schulten,K. (2005) Scalable molecular dynamics with NAMD. *J. Comput. Chem.*, **26**, 1781–1802.

20. Jarzynski,C. (1997) Nonequilibrium equality for free energy differences. *Phys. Rev. Lett.*, **78**, 2690–2693.

21. Arrar,M., Boubeta,F.M., Szretter,M.E., Sued,M., Boechi,L. and Rodriguez,D. (2019) On the accurate estimation of free energies using the Jarzynski equality. *J. Comput. Chem.*, **40**, 688–696.

22. Cleland,W.W. (1963) The kinetics of enzyme-catalyzed reactions with two or more substrates or products. I. Nomenclature and rate equations. *Biochim. Biophys. Acta.*, **67**, 104–137.

23. Rosing,J. and Slater,E.C. (1972) The value of ΔG for the hydrolysis of ATP. *Biochim. Biophys. Acta (BBA)-Bioenergetics*, **267**, 275–290.

24. Yount,R.G., Lawson,D. and Rayment,I. (1995) Is myosin a 'back door' enzyme? *Biophys. J.*, **68**, 44s–49s.

25. Sweeney,H.L. and Houdusse,A. (2010) Structural and functional insights into the myosin motor mechanism. *Annu. Rev. Biophys.*, **39**, 539–557.

26. Henn,A., Shi,S.P., Zarivach,R., Ben-Zeev,E. and Sagi,I. (2002) The RNA helicase DbpA exhibits a markedly different conformation in the ADP-bound state when compared with the ATP- or RNA-bound states. *J. Biol. Chem.*, **48**, 46559–46565.

27. El Mezgueldi,M., Tang,N., Rosenfeld,S.S. and Ostap,E.M. (2002) The kinetic mechanism of Myo1e (human myosin-IC). *J. Biol. Chem.*, **24**, 21514–21521.

28. Holdgate,G., Meek,T. and Grimley,R. (2018) Mechanistic enzymology in drug discovery: a fresh perspective. *Nat. Rev. Drug Discov.*, **17**, 115–132.

29. Pan,A., Saw,W.G., Manimekalai,M.S.S., Grüber,A., Joon,S., Matsui,T., Weiss,T.M. and Grüber,G. (2017) Structural features of NS3 of Dengue virus serotypes 2 and 4 in solution and insight into RNA binding and the inhibitory role of quercetin. *Acta Cryst.*, **73**, 402–419.

30. Gross,C.H. and Shuman,S. (1998) The nucleoside triphosphatase and helicase activities of vaccinia virus NPH-II are essential for virus replication. *J. Virol.*, **72**, 4729–4736.

31. Banroques,J., Doère,M., Dreyfus,M., Linder,P. and Tanner,N.K. (2009) Motif III in superfamily 2 'helicases' helps convert the binding energy of ATP into a high-affinity RNA binding site in the yeast DEAD-box protein Ded1. *J. Mol. Biol.*, **396**, 949–966.

32. Ye,J., Osborne,A.R., Groll,M. and Rapoport,T.A. (2004) RecA-like motor ATPases—lessons from structures. *Biochim. Biophys. Acta (BBA)-Bioenergetics*, **1659**, 1–18.